Vortex cores, strain cells, and filaments in quasigeostrophic turbulence

Mark R. Petersen[a] and Keith Julien
Department of Applied Mathematics, University of Colorado at Boulder, Boulder, Colorado 80309

Jeffrey B. Weiss
PAOS, University of Colorado at Boulder, Boulder, Colorado 80309

We present numerical simulations of decaying two-dimensional (2D) and three-dimensional quasigeostrophic (3D QG) turbulence. The resulting vorticity fields are decomposed into three components: the vortex cores, the strain cells, and the background. In 2D, the vortex cores induce five times the energy as the background, while in 3D QG the background plays a more dominant role and induces the same amount of energy as the vortex cores, quantifying previous observations that 3D QG has a more active filamentary background. The probability density function of the total velocity field is nearly Gaussian in 3D QG but significantly less so in 2D. In both 2D and 3D QG, the velocities induced by the vortex cores and the strain cells are non-Gaussian. In both 2D and 3D QG turbulence, the enstrophy spectrum of the background is close to k^{-1} predicted by inverse cascade theories. © *2006 American Institute of Physics*. [DOI: 10.1063/1.2166452]

I. INTRODUCTION

The large-scale fluid dynamics of Earth's atmosphere and oceans are strongly influenced by planetary rotation and vertical density stratification. The two–dimensional (2D) vorticity equation for barotropic turbulence and the 3D quasigeostrophic (3D QG) equation are standard models used to study the effects of rotation and stratification on large-scale turbulence. Because of its relative simplicity, 2D turbulence has, in the past, been the focus of many investigations. The question of how the behavior changes in three dimensions is of obvious importance.

The dominant behavior of freely decaying 2D turbulence is vortex formation and merger.[1–3] Numerical experiments show that an initial distribution of random vorticity coalesces into a population of small vortices, which continue to merge with like-signed partners until the field is dominated by a few large vortices. Vortex merger is the mechanism for the inverse cascade, where energy moves from smaller to larger scales. This is in contrast to isotropic 3D turbulence, where vortex stretching and tilting transfers energy from large to small scales.

The geophysically relevant three-dimensional system that is closest to 2D fluid dynamics is 3D QG. 3D QG behaves like stacked layers of 2D turbulence that communicate through baroclinic interactions. Like the 2D vorticity equation, 3D QG lacks a stretching and tilting term, so energy travels up-scale in an inverse cascade by means of vortex merger. As time progresses, like-signed vortices in neighboring layers align to form vertical columns.[4]

Here we compare decaying 2D and 3D QG vortex-dominated turbulence by decomposing the vorticity field into three separate regions: vortex cores, strain cells, and the remaining background. Previous work on partitioning the flow in 3D QG focused on the vortex component only.[5,6] Vortex-dominated turbulence can be partitioned using a variety of techniques, including the Okubo-Weiss parameter,[7–10] subjective census techniques,[11] wavelet analyses,[12–15] and time-series based methods.[16]

Partitioning the potential vorticity field allows quantitative comparison between the components of 2D and 3D QG turbulence. Qualitative observations in 2D show low, uniformly distributed vorticity content between the vortices,[17] while 3D QG is populated by a larger number of filaments that carry considerably more vorticity.[18,19] Vortex filaments in 3D QG are longer-lived than their 2D counterparts, indicating that filaments are transferred to the dissipation scale more efficiently in 2D. This difference in behavior can be qualitatively explained in terms of the Green function, which in 2D is logarithmic, and in 3D QG decays more quickly as $1/r$.[19]

Studying the statistical properties of velocity fields is an important method for quantifying turbulent flows. These statistical characteristics can be studied using *in situ* measurements, laboratory experiments, physically detailed numerical models, and idealized turbulence models. In 2D turbulence, non-Gaussian velocity probability density functions (pdfs) are due to the vortex component of the flow.[20,21] In the context of ocean turbulence, Bracco *et al.*[22] examined daily velocity data from subsurface floats in the North Atlantic and equatorial Atlantic, and found that distributions were Gaussian for small velocities but approached exponential tails for large velocities.[22] A follow-up study of the North Atlantic using high-resolution numerical simulations found non-Gaussian velocity pdfs at the surface and at 1500 m with similar kurtosis values to the *in situ* data.[23]

In this paper, we compare numerical simulations of 2D and 3D QG turbulence using a pseudospectral model with periodic boundary conditions. The paper is organized as follows: Section II details the equation set, numerical method, initial conditions, and experimental parameters. The methods

[a]Present address: Los Alamos National Laboratory, Los Alamos, NM 87545. Electronic mail: mpetersen@lanl.gov

18, 026601-1

of analysis and separation of the full vorticity field into vortex cores, strain cells, and the background are discussed in Sec. III. The results in Sec. IV show spectra, pdfs, and statistics for these components as well as a point vortex model. A derivation of the velocity pdf for a single 3D point vortex is given in the Appendix.

II. THE QUASI-GEOSTROPHIC REGIME

The QG equation, first derived by Charney,[24] is widely used to model rotating, stratified, shallow fluids like Earth's oceans and atmosphere. It is the basis for analytic models of Rossby waves, cyclogenesis, and ocean basin circulation, as well as early numerical weather forecasting models and modern turbulence models like those presented here. Quasigeostrophy results from the incompressible Navier-Stokes equation in the asymptotic limit of rapid rotation and strong stable stratification. Derivations of the QG equations can be found in many standard textbooks such as Salmon.[25]

In the QG regime, the vertical velocity is asymptotically small and the flow is horizontally nondivergent. Thus, as in 2D, 3D QG flow can be described by a streamfunction Ψ. In 2D, the dynamics are governed by the relative vorticity $\omega = \partial_x v - \partial_y u = \nabla^2_{2D}\Psi$, where ∇^2_{2D} is the 2D Laplacian operator. In 3D QG, the appropriate vorticity is the potential vorticity q. In order to elucidate the effects of three-dimensionality on inverse-cascade turbulence, we focus on the simplest extension to 2D fluid dynamics. Thus, we work on the f plane, where the Coriolis parameter f is constant, and restrict ourselves to the case where the Brunt-Väisälä frequency N is constant. It is then convenient to work in so-called stretched coordinates, where vertical length scales are stretched to make $N/f=1$. Under these conditions, the potential vorticity becomes extremely simple,

$$q = \omega + \frac{\partial^2 \Psi}{\partial z^2} = \nabla^2_{3D}\Psi, \qquad (1)$$

where ∇^2_{3D} is the 3D Laplacian operator. It will be convenient to denote the vorticity as ζ, and denote gradients and Laplacians without a subscript, where it is understood that $\zeta = \omega$ and $\nabla = \nabla_{2D}$ in 2D, and $\zeta = q$ and $\nabla = \nabla_{3D}$ in 3D QG.

The dynamical vorticity equation is then the same for both 2D and 3D QG,

$$\frac{D\zeta}{Dt} \equiv \frac{\partial \zeta}{\partial t} + J(\Psi, \zeta) = \mathcal{D}\zeta, \qquad (2)$$

where D/Dt is the horizontal material derivative for both 2D and 3D QG and can be written in terms of the horizontal Jacobian $J(\Psi, \zeta) = \partial_x \Psi \partial_y \zeta - \partial_y \Psi \partial_x \zeta$, and $\mathcal{D}$ is an appropriate dissipation operator. Note that because there is no vertical velocity in 3D QG, the advection operator is strictly horizontal in both 2D and 3D QG. The system is closed by the vorticity-streamfunction relation,

$$\zeta = \nabla^2 \Psi, \qquad (3)$$

where ∇^2 is the 2D or 3D Laplacian for 2D or 3D QG flow, respectively. Written this way, the equations for 2D and 3D QG look identical, but the 3D Laplacian in the 3D QG

vorticity-streamfunction relation provides a coupling between horizontal levels that is absent in 2D.

The vorticity-streamfunction relation can be inverted in terms of a Green function $G(\mathbf{x})$

$$\Psi(\mathbf{x}) = \int G(\mathbf{x} - \mathbf{x}')\zeta(\mathbf{x}')d\mathbf{x}', \qquad (4)$$

where $G_{2D} \sim \log r$ and $G_{3D} \sim 1/r$. Using the Green function formulation allows all quantities to be represented in terms of the vorticity field. The velocity field, for example, can be considered to be induced by the vorticity field through derivatives of the Green function. Two inviscid invariants that play an important role in the turbulence are the energy E and the enstrophy Z. In terms of the vorticity field, the energy is

$$E = \frac{1}{2\mathcal{V}} \int |\nabla \Psi|^2 d\mathbf{x} = -\frac{1}{2\mathcal{V}} \int \zeta(\mathbf{x})G(\mathbf{x} - \mathbf{x}')\zeta(\mathbf{x})d\mathbf{x}d\mathbf{x}' \qquad (5)$$

and the enstrophy is

$$Z = \frac{1}{2\mathcal{V}} \int \zeta^2(\mathbf{x})d\mathbf{x}, \qquad (6)$$

where $\mathcal{V}$ is the volume of the fluid.

III. SEPARATION OF THE POTENTIAL VORTICITY FIELD

In vortex-dominated turbulence such as decaying 2D and 3D QG turbulence, the structures that dominate the flow are vorticity structures. It is thus appropriate to decompose the flow based on a partition of the vorticity field,

$$\zeta(\mathbf{x}) = \sum_i \zeta_i(\mathbf{x}), \qquad (7)$$

where the subscript represents the component of the partition. The simplest type of partition, which we use here, results from cutting physical space into nonoverlapping sets with each point in space $\mathbf{x}$ having, at most, only one nonzero component. Note, however, that some decomposition techniques, such as wavelet-based techniques, naturally allow each point in space to have multiple nonzero components. One advantage of using a nonoverlapping or an orthogonal partition is that the enstrophy decomposes simply into a sum of enstrophy components, $Z = \Sigma_i Z_i$, with

$$Z_i = \frac{1}{2\mathcal{V}} \int \zeta_i^2(\mathbf{x})d\mathbf{x}. \qquad (8)$$

The energy decomposition is more complex. Each component gives rise to a self-energy E_i,

$$E_i = -\frac{1}{2\mathcal{V}} \int \zeta_i(\mathbf{x})G(\mathbf{x} - \mathbf{x}')\zeta_i(\mathbf{x})d\mathbf{x}d\mathbf{x}', \qquad (9)$$

and, in addition, there is an interaction energy E_{ij} between components i and j,

$$E_{ij} = -\frac{1}{\mathcal{V}} \int \zeta_i(\mathbf{x}) G(\mathbf{x} - \mathbf{x}') \zeta_j(\mathbf{x}) d\mathbf{x} d\mathbf{x}'. \tag{10}$$

The total energy is then the sum of all self-energies and interaction energies.

In 2D turbulence, it is useful to partition the vorticity field into vortex cores, strain cells, and the remaining background which contains the filaments.[9,17,21] Qualitatively, vortex cores have high vorticity magnitude and are roughly elliptical in shape. The flow induced by a vortex core is similar to that of a point vortex, a delta function in vorticity. A strain cell, also called a circulation cell, is an annular region with high shear that surrounds each vortex core. The background is what remains after removing the cores and the strain cells and contains long, thin vortex filaments that are stretched until they reach the dissipation scale and are dissipated. Qualitative visualizations indicate that the same decomposition may be useful in 3D QG.

As discussed in the Introduction, there are many quantitative methods to partition a complex vorticity field. Here we choose a simple method based on thresholds in the Okubo-Weiss parameter. This has the decided advantage of simplicity and allows the same method to be used in both 2D and 3D QG. Another advantage of the Okubo-Weiss parameter is that it is, apart from a factor of 4, identical to a parameter often used to identify structures in isotropic 3D turbulence.

The quantity known as λ_2, the middle eigenvalue of a tensor of velocity gradients, is often used to quantify and visualize coherent structures in fully 3D turbulence.[26] Isosurfaces of λ_2 identify vortex rings and jets in complex 3D

simulations. Here we show that in 2D and 3D QG, the Okubo-Weiss parameter OW $= 4\lambda_2$. Physically, these parameters measure the relative contribution of vorticity versus strain. The Okubo-Weiss parameter, developed in the context of ocean modeling and 2D hydrodynamics,[7,8] is negative where rotation dominates and positive where strain dominates. The relationship between the Okubo-Weiss parameter and λ_2 is discussed in Ref. 27 and is briefly reviewed here.

The Okubo-Weiss parameter is

$$OW = S^2 - \omega^2 \tag{11}$$

$$= s_n^2 + s_s^2 - \omega^2 \tag{12}$$

$$= 4\left[\left(\frac{\partial u}{\partial x}\right)^2 + \frac{\partial u}{\partial y}\frac{\partial v}{\partial x}\right], \tag{13}$$

where ω is the relative vorticity and S, the strain, is composed of a normal component $s_n = \partial_x u - \partial_y v$ and a shear component $s_s = \partial_y u + \partial_x v$. The λ_2 parameter is the middle eigenvalue of the symmetric tensor $\mathbf{S}^2 + \mathbf{\Omega}^2$, where $\mathbf{S}$ and $\mathbf{\Omega}$ are the symmetric and antisymmetric parts of the velocity gradient tensor $\nabla \mathbf{u}$; i.e., $S_{ij} = 1/2(u_{i,j} + u_{j,i})$ and $\Omega_{ij} = 1/2(u_{i,j} - u_{j,i})$, and the comma notation indicates partial derivatives. For a 3D velocity field, $\mathbf{S}^2 + \mathbf{\Omega}^2$ is a 3×3 matrix at each grid point, and the eigenvalues are ordered such that $\lambda_1 \geq \lambda_2 \geq \lambda_3$.

In 3D QG, the fluid is incompressible and the vertical velocity is asymptotically small. These assumptions simplify $\mathbf{S}^2 + \mathbf{\Omega}^2$ considerably so that its leading-order eigenvalues are

$$\lambda = \left\{\left(\frac{\partial u}{\partial x}\right)^2 + \frac{\partial u}{\partial y}\frac{\partial v}{\partial x}, \frac{1}{2}\left[\left(\frac{\partial u}{\partial x}\right)^2 + \frac{\partial u}{\partial y}\frac{\partial v}{\partial x}\right] \pm \frac{1}{2}\sqrt{\left[\left(\frac{\partial u}{\partial x}\right)^2 + \frac{\partial u}{\partial y}\frac{\partial v}{\partial x}\right]^2 + \left(\frac{\partial u}{\partial x}\frac{\partial v}{\partial z} - \frac{\partial u}{\partial z}\frac{\partial v}{\partial x}\right)^2 + \left(\frac{\partial u}{\partial y}\frac{\partial v}{\partial z} - \frac{\partial u}{\partial z}\frac{\partial v}{\partial y}\right)^2}\right\}. \tag{14}$$

Simple inequalities show that the middle eigenvalue is always

$$\lambda_2 = \left(\frac{\partial u}{\partial x}\right)^2 + \frac{\partial u}{\partial y}\frac{\partial v}{\partial x} \tag{15}$$

and that $\lambda_1\lambda_3 < 0$.

For the 2D vorticity equation, all terms with z derivatives are zero, so (14) simplifies to

$$\lambda = \left\{0, \left(\frac{\partial u}{\partial x}\right)^2 + \frac{\partial u}{\partial y}\frac{\partial v}{\partial x}, \left(\frac{\partial u}{\partial x}\right)^2 + \frac{\partial u}{\partial y}\frac{\partial v}{\partial x}\right\}. \tag{16}$$

In this case, $\mathbf{S}^2 + \mathbf{\Omega}^2$ is really a 2×2 matrix with two equal eigenvalues. The expressions for λ_2 in 2D and 3D QG are identical, and are one-fourth the value of the Okubo-Weiss measure traditionally used in 2D turbulence studies, i.e., $\lambda_2 = 1/4\text{OW}$.

Figure 1 shows a closeup view of several vortices at time 15 in a 3D QG simulation (see Sec. IV for details), with the corresponding λ_2 field normalized by σ_ω, the standard devia-

tion of the relative vorticity, equal to the square-root of twice the relative enstrophy. The λ_2 value measures strain squared minus vorticity squared. Vortex cores, where the vorticity magnitude is large but the velocity is near zero, have large negative λ_2. The strain cells are rings of high velocity induced by the vortex cores where λ_2 is large and positive. These regions have lower vorticity than the cores and high shear strain due to the way velocity decreases with distance from the core. Areas with small $|\lambda_2/\sigma_\omega|$ are neither vortex cores nor strain cells, and include the low-vorticity filamentous structures that fill the majority of the vorticity field. Notice that for periodic boundary conditions (and for infinite domains where boundary terms vanish), λ_2 has the property in both 2D and 3D QG that the integral over each horizontal level of strain squared equals that of vorticity squared, and thus the integral of λ_2 is zero. This fact motivates the use of σ_ω to normalize λ_2.

The boundaries between vortex cores and circulation cells may be defined by the sharp transition between large
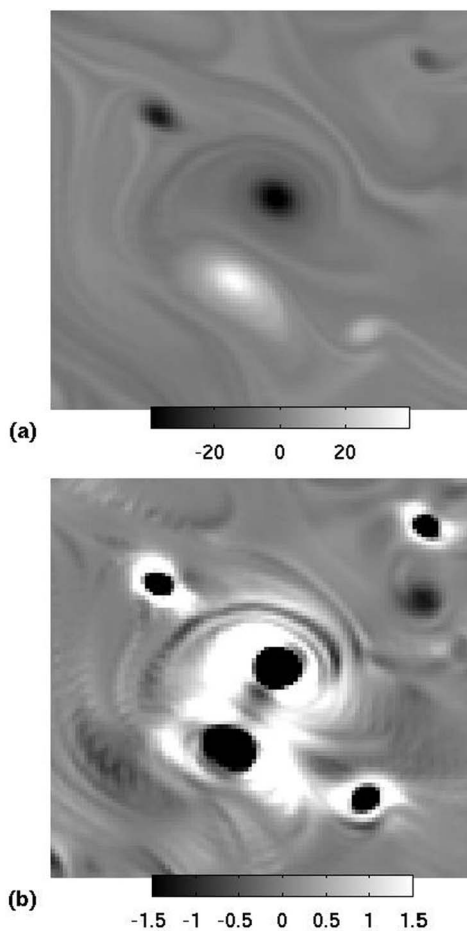
(a)

(b)

FIG. 1. A closeup view of a horizontal 3D QG plane (a) and the corresponding λ_2 field (b). Color bar values on (b) are λ_2/σ_ω, where σ_ω is the standard deviation of the relative vorticity.

(a)

(b)

FIG. 2. Energy due to portion of the potential vorticity field where λ_2/σ_ω $\leq$ critical λ_2 (solid line) and where $\lambda_2/\sigma_\omega >$ critical λ_2 (dashed line) for experiments 2D-3 (a) and 3D-2 (b) at time 15. The dotted line shows the energy in the cross term.

positive and large negative values of λ_2. Other methods of defining the vortex edge include isolines of maximum kinetic energy and maximum vorticity gradient. In atmospheric data, isolines of maximum kinetic energy show a close correspondence to $\lambda_2=0$, while isolines of maximum vorticity gradient do not strictly coincide.[28] We choose to partition the vorticity field using λ_2 (Okubo-Weiss) because it provides a straightforward measure that has been widely used in the literature. Our goal is to produce a simple, relatively robust decomposition.

In order to partition the vorticity field, we need to choose threshold values of λ_2/σ_ω. We wish to choose critical values that give decompositions that are relatively insensitive to the exact value of the threshold. To investigate the sensitivity, we calculate the energy partition as a function of critical λ_2/σ_ω. We first partition the vorticity field into two components: $\zeta_- = \{\zeta \,|\, \lambda_2/\sigma_\omega \leq \lambda_{2crit}\}$ and $\zeta_+ = \{\zeta \,|\, \lambda_2/\sigma_\omega > \lambda_{2crit}\}$. Figure 2 shows the self-energy fraction of both components along with interaction energy or cross-term. (The details of the simulations are described in Sec. IV.) As λ_{2crit} increases from negative infinity, ζ_- increasingly captures more of the vortex cores until, as λ_{2crit} approaches zero, ζ_- starts to also capture parts of filaments that we would like to include in the background. On the other hand, as λ_{2crit} decreases from positive infinity, ζ_+ increasingly captures more of the strain cells until
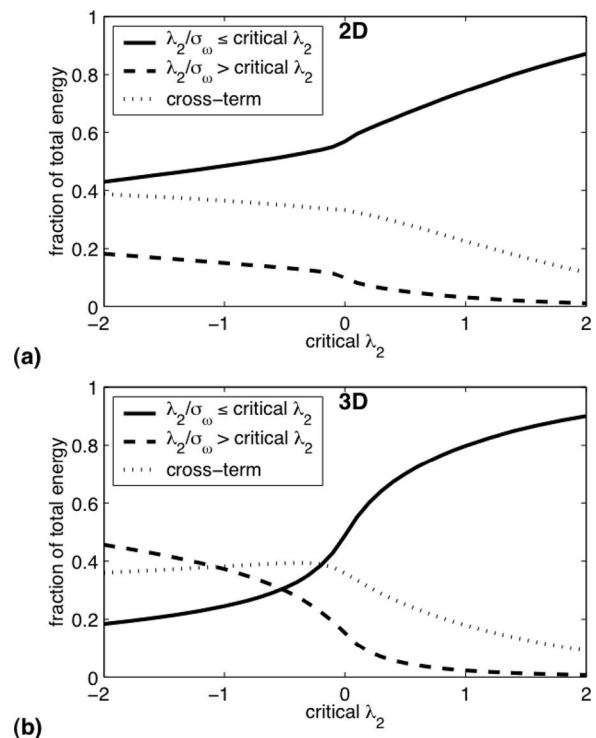
it starts including parts of the field that we, again, would like to include in the background. Thus λ_{2crit} defines precisely where we draw the boundary between cores/strain cells and background.

Figure 2 shows that, in both 2D and 3D QG, there is a region of λ_{2crit} where the energy of the components varies smoothly and relatively slowly, and then, as λ_{2crit} approaches zero, the energies change more dramatically. We investigated a range of λ_{2crit} and found that the broad features we describe here are robust to modest changes in the threshold. Here we present results for a threshold choice of $\lambda_{2crit}=\pm 1$.

IV. NUMERICAL SIMULATIONS

We numerically integrate Eqs. (2) and (3) using a pseudospectral numerical model with Fourier basis functions in a 2D and 3D periodic box. The nonlinear advective terms are computed in physical space and then transformed to spectral space using a standard two-thirds rule to prevent aliasing. The time-stepping scheme is a third-order Runge-Kutta with implicit/explicit operator splitting[29] that minimizes the storage of large arrays. We use hyperviscous dissipation, $\mathcal{D}=-\nu\nabla^4$, which preferentially dissipates higher wavenumber modes, and allows us to achieve more inviscid behavior at the larger scales of interest while retaining the dissipation necessary for numerical stability at small scales.

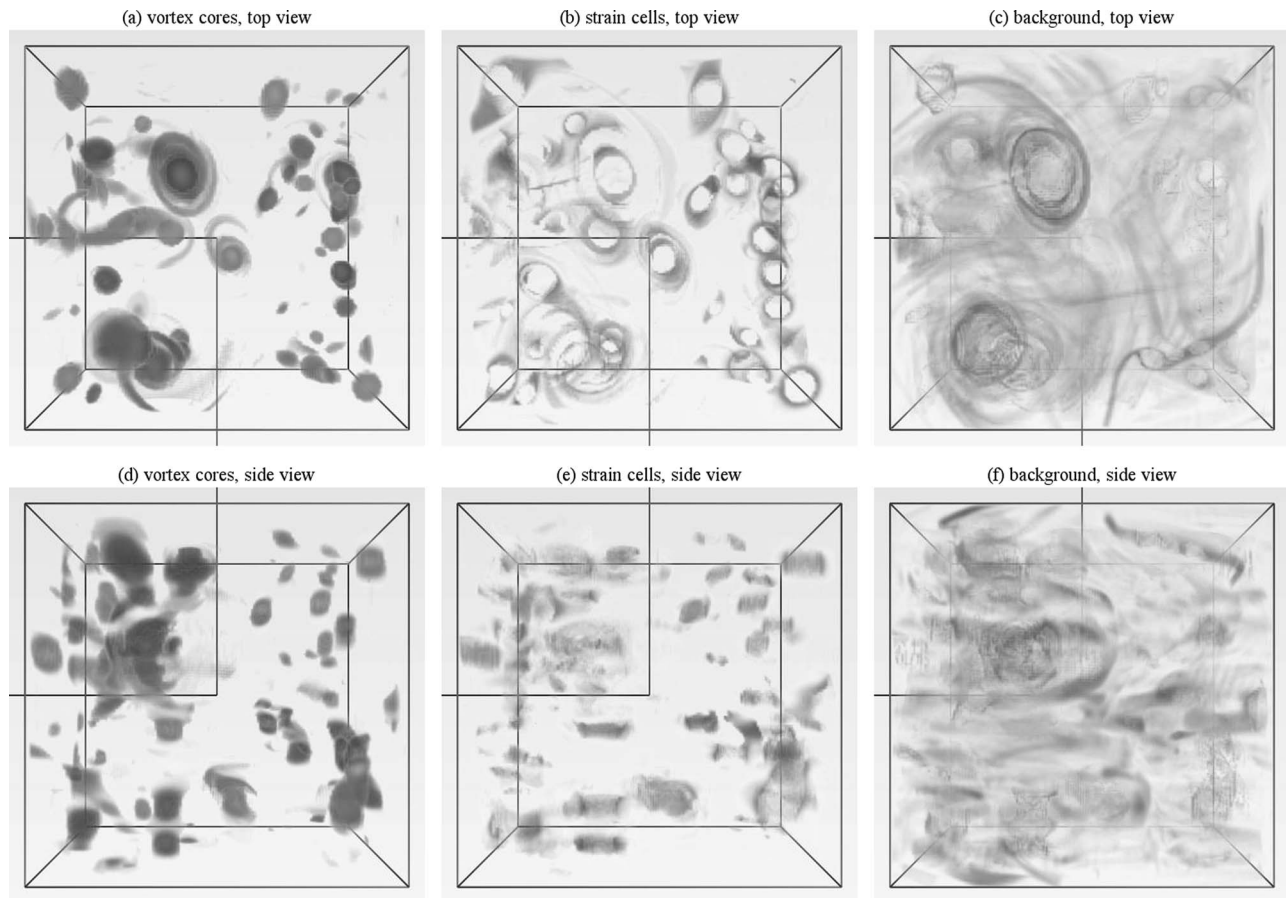The initial condition is obtained from the energy spectrum

FIG. 3. Volume-rendered images of the vortex cores, strain cells, and background in 3D QG at time 15. Transparent (light) areas have potential vorticity near zero, while opaque (dark) areas have larger potential vorticity magnitude. Colors are scaled to the maximum magnitude in each field. The block shown is a 128^3 grid point subvolume of a 512^3 simulation.

$$E(k) = \frac{E_0 k^6}{\left(1 + \dfrac{k}{60}\right)^{18}} \tag{17}$$

with random phases. This initial spectrum, which was used in previous studies of 2D turbulence,[21,11] is a narrowband spectrum that peaks at $k=30$. The constant E_0 is chosen such that the initial total energy is 1, which sets the time scale of the evolution.

The simulations were carried out at a resolution of 512^2 grid in 2D and 512^3 in 3D QG. Here we present simulations with $\nu_{2D} = 5 \times 10^{-9}$ and $\nu_{3D\,QG} = 2.5 \times 10^{-9}$. Solutions with other values of viscosity were also computed and confirm the results reported here. The behavior in 2D as viscosity is varied is discussed in Bracco et al.[21] The viscosity choice for 3D QG is the highest possible without significant buildup of energy at the highest wave numbers. The 2D case was repeated ten times to reduce the sampling variability relative to the larger number of grid points in 3D. Each of the ten repetitions used identical parameters and initial energy spectra, but differed in their random initial phases.

The general evolution for these flows is well known.[2,4] Around time five (based on unit initial energy), coherent vortices self-organize. As time progresses, the vortices interact, and the vortex population evolves in a self-similar manner. In this work, we wish to investigate the components of the

vorticity field in the self-similar evolution regime. Following Bracco et al.,[21] we choose time $t=15$ for our analyses.

The vorticity field ζ is decomposed into three components: the vortex cores ζ_c, the strain cells ζ_s, and the background ζ_b, where

$$\zeta_c(\mathbf{x}) = \begin{cases} \zeta(\mathbf{x}), & \lambda_2/\sigma_\omega < -\lambda_{2\mathrm{crit}} \\ 0, & \lambda_2/\sigma_\omega \geqslant -\lambda_{2\mathrm{crit}} \end{cases},$$

$$\zeta_b(\mathbf{x}) = \begin{cases} \zeta(\mathbf{x}), & -\lambda_{2\mathrm{crit}} \leqslant \lambda_2/\sigma_\omega \leqslant \lambda_{2\mathrm{crit}} \\ 0, & \text{otherwise} \end{cases},$$

$$\zeta_s(\mathbf{x}) = \begin{cases} 0, & \lambda_2/\sigma_\omega \leqslant \lambda_{2\mathrm{crit}} \\ \zeta(\mathbf{x}), & \lambda_2/\sigma_\omega > \lambda_{2\mathrm{crit}} \end{cases}. \tag{18}$$

The decomposition is shown in Fig. 3, which contains volume-rendered images of the potential vorticity components in 3D QG. The vortex cores, where the vorticity is stronger than the shear, tend to align in columns, as expected.[4] A strain cell forms a ring around each core, but is not as tall as the core itself. The background, which contains 85% of the grid points, has filamentary structures that spiral out from the strain cells and are large in horizontal extent.

The pdfs of ζ, shown in Fig. 4, provide insight into the decomposition. The picture that emerges is similar for 2D and 3D QG. The large-vorticity tails are due to the vortex
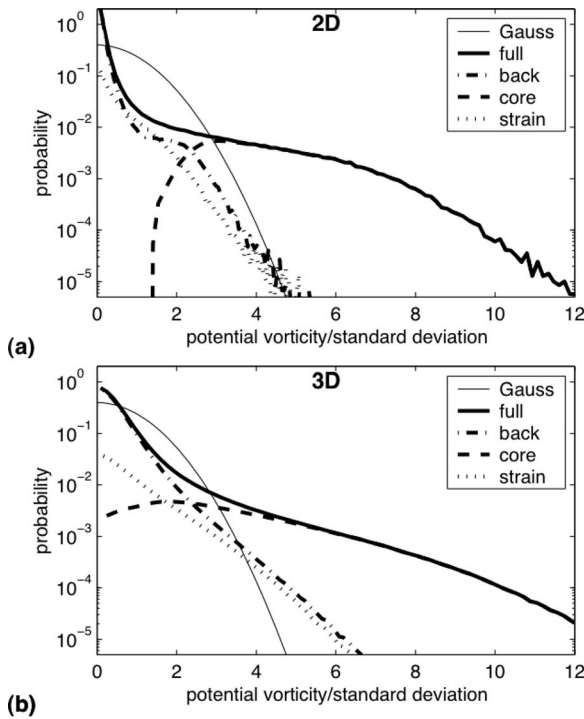
FIG. 4. Pdfs of vorticity of the full field (solid line), the vortex cores (dashed line), the strain cells (dotted line), and the background (dash-dot) at time 15 for 2D (a) and 3D QG (b). All pdfs are normalized by the standard deviation of the full field. A Gaussian distribution (thin line) with the same standard deviation is superimposed.
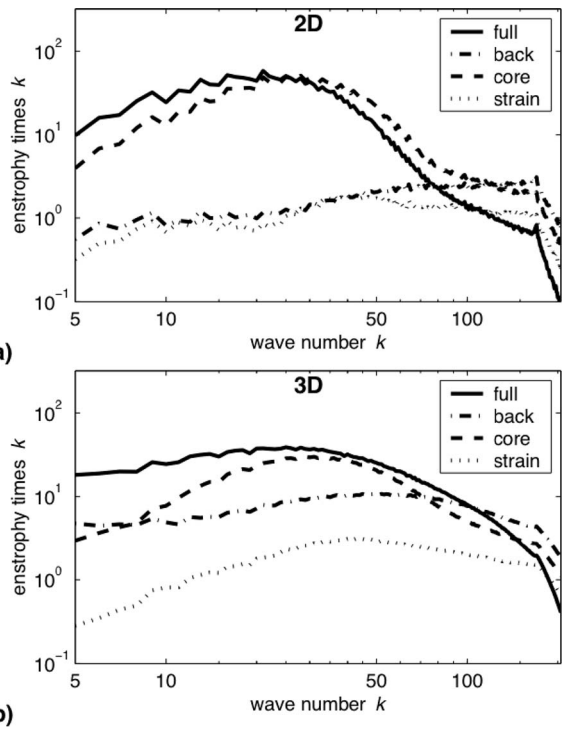

FIG. 5. Compensated enstrophy spectrum of the full field (solid line), the vortex cores (dashed line), the strain cells (dotted line), and the background (dash-dot) at time 15 for 2D (a) and 3D QG (b). Inverse cascade theories predict slopes of k^{-1}, which is horizontal on these plots.

cores, and the region near zero vorticity is due to the background. The strain cells do not appear as strikingly different from the background in either 2D or 3D QG except for their small contribution very near zero. This is not surprising, as strain cells are regions of high velocity around the vortices, where the vorticity level is similar to the background. These results are consistent with previous interpretations of highly non-Gaussian vorticity pdfs; the vorticity accessible to turbulent interactions in the background decays quickly, while the vorticity protected within isolated vortices persists.[2] The 3D vorticity pdfs are smoother because there are more sample points (512^3) than in the 2D case (10×512^2).

The compensated enstrophy spectra, Fig. 5, show significant differences among the components. The classical enstrophy spectrum slope for 2D and 3D QG turbulence is k^{-1} in the inertial range.[30–32] Compensating the spectra by multiplying by k renders curves following the classical slope horizontal, which is easier for the human eye to discern. The full fields in both 2D and 3D QG have steeper spectra than the classical prediction. A previous wavelet-based decomposition in 2D found that the steeper spectrum was due to the vortices, with the background and strain cells, grouped together in that decomposition, following the classical scaling.[13] Here, we see that in 2D both the background and strain cells are approximately k^{-1} with the cores giving a steeper slope. In 3D QG, the background and strain cells are closer to k^{-1} than the cores, but not as close as in 2D. Note that the shape of the spectra of the cores is very similar in 2D and 3D QG.

The time evolution of the fraction of the enstrophy in the

components is seen in Fig. 6. In both 2D and 3D QG, the fraction of enstrophy in the cores grows until it carries the majority of the enstrophy, and the strain cells carry relatively little enstrophy. However, there is a major difference in that
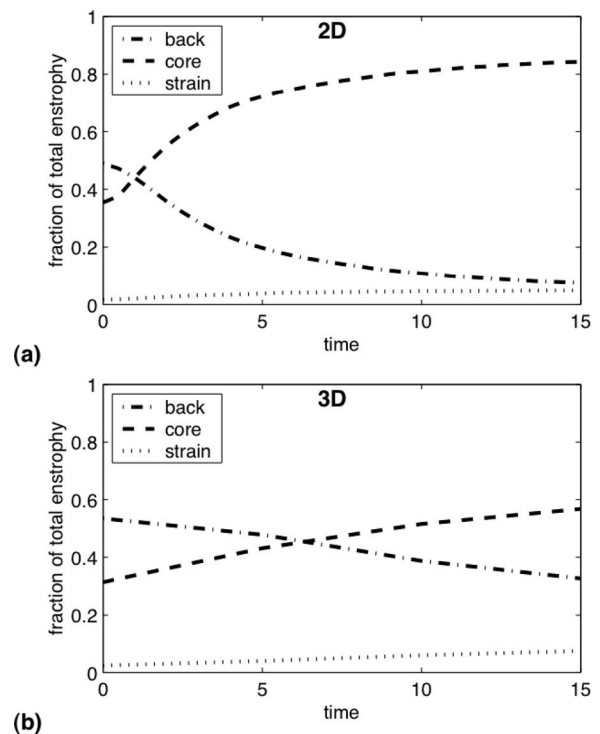

FIG. 6. Enstrophy of the vortex cores (dashed line), the strain cells (dotted line), and the background (dash-dot) as a function of time for 2D (a) and 3D QG (b).

the background in 3D QG carries significantly more of the enstrophy than in 2D. Indeed, at time $t=15$, the fraction of enstrophy in the background in 3D QG is 4.3 times more than in 2D, while the cores in 3D QG carry 67% of the fractional enstrophy of the cores in 2D. This quantifies the previous observation that the filaments in the background are more active in 3D QG than in 2D.[19]

Because we use a partition that is local in vorticity, the decomposition in terms of vorticity and enstrophy is relatively simple. In contrast, the velocity and energy induced by a component are global due to the integrative effect of the Green function. As a result, the velocity at each point in space has a contribution from each of the components and the energy is the sum of self-energies [Eq. (9)] and interaction energies [Eq. (10)]. Here we group all the interaction energies together and decompose the total energy into

$$E = E_c + E_b + E_s + E_i, \tag{19}$$

where subscripts c, b, and s denote the self-energy of the cores, background, and strain cells, respectively, and subscript i denotes the sum of the interaction energies.

The time evolution of the energy decomposition is seen in Fig. 7. In both 2D and 3D QG, the self-energy of the background decays with time, and the self-energy of the strain cells is relatively small. However, there are several significant differences. In 2D the core self-energy is the largest component after vortex formation, and by time 15 the background self-energy is less than 10% of the total. In 3D QG, the core self-energy is always smaller than the background self-energy, although they are nearly equal by time 15, when the background self-energy still contributes over 25% of the total. Further, while the total interaction energy is large in 2D, it is always less than the core self-energy. In contrast, the total interaction energy is the largest component of 3D QG, contributing nearly half the total energy by time 15.

The pdf of velocity is a quantity that is often used to characterize turbulence. Non-Gaussian velocity pdfs have been found in collections of 2D point vortices,[20] 2D turbulence,[21] high-resolution ocean models,[23] and ocean data.[22] Here we investigate the velocity pdf in 3D QG and look at how the different components contribute.

The velocity pdfs at time 15 are seen in Fig. 8, where each pdf is scaled to have unit variance. In both 2D and 3D QG, the velocities induced by the cores and strain cells are similarly non-Gaussian, while the velocity induced by the background and the full field are very similar and more Gaussian. In 2D the background-induced and total velocities are non-Gaussian, while in 3D QG they are very close to Gaussian. Interpreting this decomposition is not straightforward. The total velocity at each point in space is the sum of the velocities induced by each component. Further, while scaling the variance to unity makes slopes easy to compare, it exaggerates the effect of the components with small velocities.

The kurtosis of a pdf, the ratio of the fourth moment to the square of the second moment, gives a quantitative indication of the degree of Gaussianity; a Gaussian pdf has a kurtosis of 3. The time evolution of the kurtosis is seen in
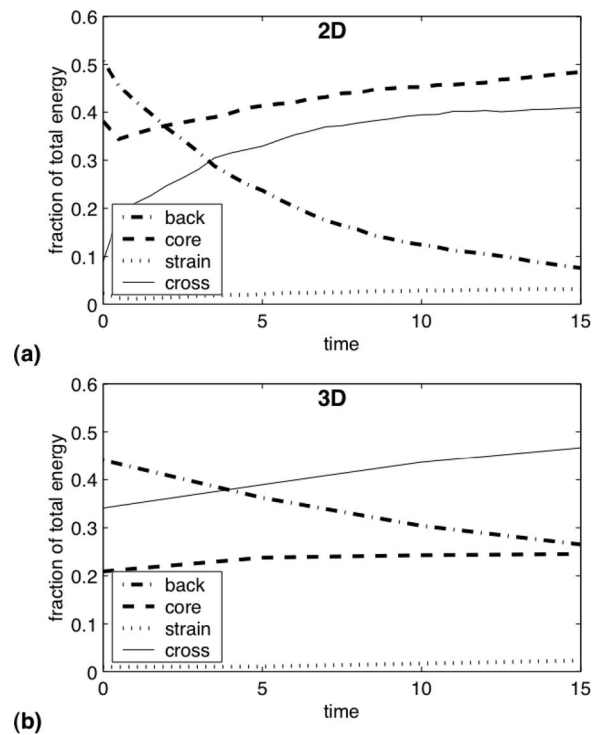

FIG. 7. Self-energies induced by the vortex cores (dashed line), the strain cells (dotted line), the background (dash-dot), and the sum of the interaction energies (solid line), as a function of time, for 2D (a) and 3D QG (b).

Fig. 9. In 2D, the kurtosis of the strain cells grows quickly and remains relatively constant after vortex formation. The kurtoses of the cores, background, and full field grow more smoothly, and by $t=15$ all are greater than 3, in agreement with the pdfs in Fig. 8. The kurtosis curves in 3D QG are very different, with the kurtoses of the background and full field remaining very close to 3, the kurtosis of cores growing smoothly to a value larger than in 2D, and the kurtosis of the strain cells dropping rapidly from large values. Thus, we again see that in 3D QG the background-induced and total velocities are more Gaussian than 2D. Further, it appears that the total velocity in 3D QG is strongly influenced by the Gaussian background-induced velocity. In 2D, on the other hand, the kurtosis indicates that the total velocity field is less Gaussian than the background, indicating that other components significantly affect the total. This is consistent with the previous observation that the background contains much more energy in 3D QG than in 2D, and thus has a stronger influence on the full behavior.

In 2D, at lower Reynolds numbers the velocity pdf is Gaussian, and transitions to a non-Gaussian pdf at higher Reynolds numbers.[21] We performed an additional simulation of 3D QG at $\nu_{3D\,QG}=5\times10^{-10}$, or five times higher Reynolds number than discussed above. This simulation still shows Gaussian velocity pdfs but is clearly under-resolved and thus will not be discussed further. It is possible that at even higher Reynolds numbers, velocity pdfs in 3D QG become non-Gaussian; here we can only conclude that at similar resolutions the velocity in 3D QG is more Gaussian than in 2D.

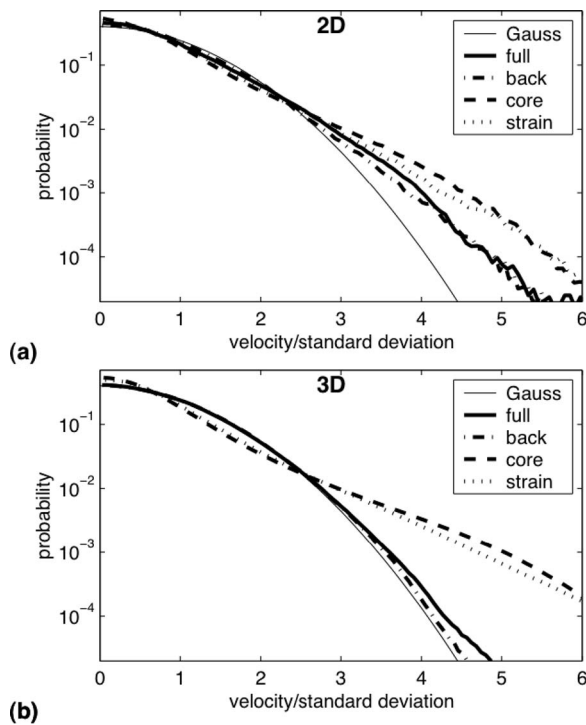In both 2D and 3D QG, the velocity imposed by the

FIG. 8. Pdfs of velocity induced by the full field (solid line), the vortex cores (dashed line), the strain cells (dotted line), and the background (dash-dot) at time 15 for 2D (a) and 3D QG (b). Each pdf has a standard deviation of 1. A Gaussian distribution (thin line) with a standard deviation of 1 is superimposed.
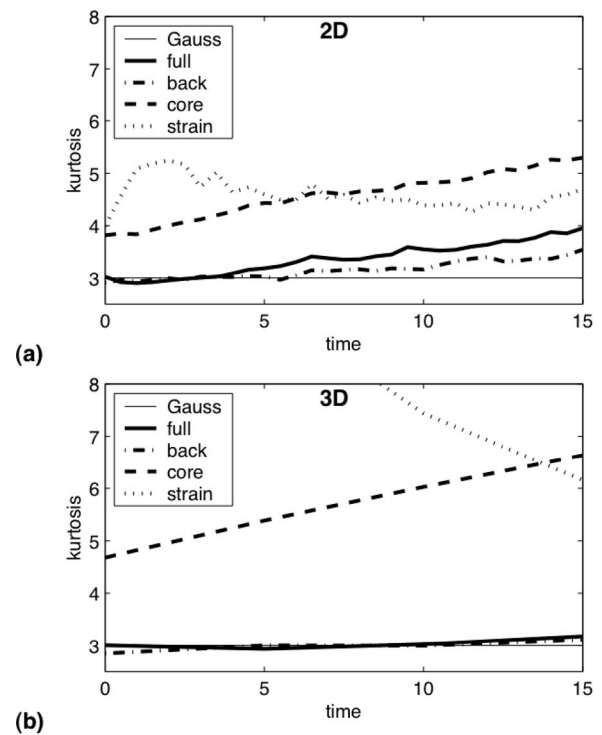

FIG. 9. Kurtosis of velocity fields induced by the full field (solid line), the vortex cores (dashed line), the strain cells (dotted line), and the background (dash-dot) as a function of time for 2D (a) and 3D QG (b). A Gaussian distribution has a kurtosis of 3 (thin line).

vortex cores is non-Gaussian. Vortex cores are compact regions of strong vorticity which induce velocity fields over large distances. The idealization where the size of the core goes to zero while keeping the circulation constant is the well-known point vortex approximation. It is thus natural to attempt to understand the non-Gaussian nature of the core-induced velocity by investigating a point vortex model.

A point vortex, also known as a singular vortex or discrete vortex element, is a delta function in the vorticity field whose Green function is the streamfunction (because $q = \nabla^2 \Psi$). In 2D, a single point vortex has a velocity field whose pdf decays as $1/|\mathbf{u}|^3$, and hence has a variance that diverges logarithmically. The velocity induced by a random collection of N such point vortices slowly converges to a Gaussian as N goes to infinity, and remains significantly non-Gaussian for N comparable to that seen in the kind of turbulent flows studied here.[33,20] In 3D QG, a point vortex with circulation Γ induces a horizontal velocity field

$$\mathbf{u} = (u,v) = \frac{\Gamma(y,-x)}{4\pi|\mathbf{x}|^3}. \tag{20}$$

This is identical to the Bio-Savart rule used in electromagnetics for the magnetic field produced by an electric current in a vertically oriented wire. The pdf of the horizontal velocity induced by a single randomly placed 3D QG point vortex p_1 scales as $p_1 \sim |\mathbf{u}|^{-2.5}$, as shown in the Appendix.

We are interested in the velocity induced by a collection of such point vortices. If the pdf for a single variable, p_1, scales as $p_1 \sim |\mathbf{u}|^{-\alpha}$, then the pdf for a sum of such variables

p falls into one of three classes depending on α. If $\alpha > 3$, then p_1 has finite variance, and by the central limit theorem p converges quickly to a Gaussian. If $\alpha = 3$, as in the 2D case, the variance of p_1 diverges logarithmically and p converges slowly to a Gaussian. If $1 < \alpha < 3$, which is the case for isotropic 3D[33] and 3D QG, the variance of p_1 diverges and p converges to a Lévy law. Analytic formulas are only known in the case where $\alpha = 2$ and $\alpha = 3$ (see Ref. 34, p. 83). In general, Lévy laws have power-law tails that contain a much larger proportion of high velocity events than Gaussian distributions. Thus, the non-Gaussian core-induced velocity is consistent with the velocity induced by 3D QG point vortices.

V. CONCLUSIONS

We have decomposed the vorticity field in numerical simulations of decaying 2D and 3D QG turbulence into vortex cores, strain cells, and the remaining background using a simple threshold in the Okubo-Weiss parameter. We have shown that the Okubo-Weiss parameter, commonly used to identify structures in 2D, is, in 2D and 3D QG, equivalent (apart from a constant) to the middle eigenvalue used to identify structures in isotropic 3D turbulence.

In both 2D and 3D QG, the enstrophy spectra for the background and strain cells are close to the k^{-1} slope predicted by traditional inverse cascade theories. The spectra for the cores and the full field are significantly steeper, indicating that the cores slow down the inverse cascade.

The most striking difference between 3D QG and 2D is the strength of the background in 3D QG, which takes the

form of active filaments. The fractional enstrophy contained in the background at $t=15$ is 4.3 times larger in 3D QG than in 2D, and corresponding ratio of fractional self-energies is 3.5. Indeed, in 2D the background enstrophy and self-energy are nearly negligible, which has led many researchers to model 2D turbulence as a single component fluid composed of a collection of vortices. The high activity of the filamentary background in 3D QG indicates that this approach may not be as successful as in 2D, and such models may require the inclusion of an active population of filaments. While models of vortices in the form of point vortices are well known and have been extensively studied, models of filaments such as vortex sheets of finite extent are much less well explored.

The different components induce velocity fields with differing properties. The vortex cores induce velocity fields with non-Gaussian pdfs, indicating the enhanced likelihood of finding large velocities, in agreement with the velocity pdf induced by 2D and 3D QG point vortex models. The background induces a velocity field that is closer to Gaussian, with a more Gaussian pdf in 3D QG than in 2D. The stronger background in 3D QG results in its Gaussian nature dominating the total velocity field, producing a Gaussian total velocity pdf.

The study of velocity pdfs in turbulent flow is relevant to parametrizations of particle dispersion in ocean modeling. Many parametrizations by linear stochastic process or eddy-diffusivity assume Gaussian velocity distributions, so that the variance of velocity data can be used to estimate turbulent diffusivity.[35,36] Several recent studies have incorporated non-Gaussian effects into particle dispersion models.[37,38] Pasquero *et al.*[39] introduced a two-process stochastic model that accounts for the presence of non-Gaussian velocity distributions by coherent vortices.

Physical data from ocean floats[22] and numerical models of the North Atlantic[23] both indicate that large-scale ocean circulation has non-Gaussian velocity pdfs with kurtosis values that are often greater than 5. In our numerical simulations, kurtosis values in this range were found only in field-induced vortex cores or strain cells. The velocity kurtosis of the total field was less than 4 for 2D turbulence and close to 3 for 3D QG turbulence. The high kurtosis values for velocity pdfs of ocean measurements indicates that these regions of the ocean may have a more dominant vortex population than the decaying 3D QG simulations presented here. In addition, the flows may be more barotropic, and hence closer to the 2D simulations than the 3D QG simulations.

Here we have focused on the Eulerian behavior of the turbulence. In recent work, Bracco *et al.*[19] found that the Lagrangian dynamics of passively advected tracers in 3D QG is very similar to that of 2D. Their Lagrangian measurements, including absolute dispersion, relative dispersion, and finite-time Lyoponov exponent, were nearly identical for 2D and 3D QG simulations, indicating that the three-dimensionality of the QG vortices, and the enhanced activity of the filaments, do not play a large role in Lagrangian dispersion. In light of the findings presented here, this may indicate that Lagrangian dispersion and mixing properties are mainly controlled by the vortex cores. If Lagrangian disper-

sion and mixing were strongly affected by the filaments, there should be significant differences in the dispersion and mixing statistics between 3D QG and 2D simulations, but this was not observed.

There are numerous idealizations in the turbulence model used here, including lack of boundary effects and thermodynamics. The experiments conducted in this study were all freely decaying, and lacked the injection of energy that the real ocean receives through boundary forcing and solar-driven advection. The strongly non-Gaussian velocity fields found in *in situ* measurements and physically based ocean models may indicate that forced turbulence produces stronger vortices and weaker filaments than those that we have observed in freely decaying turbulence models.

APPENDIX: POINT VORTEX VELOCITY DISTRIBUTION IN 3D QG

The velocity induced by a single 3D QG point vortex located at the origin is

$$(u,v) = -\frac{\Gamma}{4\pi}\frac{(-y,x)}{(x^2+y^2+z^2)^{3/2}} \tag{A1}$$

which has magnitude

$$|\mathbf{u}| = \frac{\Gamma}{4\pi}\frac{\sqrt{x^2+y^2}}{(x^2+y^2+z^2)^{3/2}}. \tag{A2}$$

Introducing spherical coordinates (r,θ,ϕ) where $x=r\sin\phi\cos\theta$, $y=r\sin\phi\sin\theta$, and $z=r\cos\phi$, the velocity magnitude is

$$|\mathbf{u}| = \frac{\Gamma}{4\pi}\frac{\sin\phi}{r^2} \tag{A3}$$

so that lines of constant speed $|\mathbf{u}|$ are parametrized by $\phi \in [0,\pi]$, $\theta \in [0,2\pi]$ and are given by
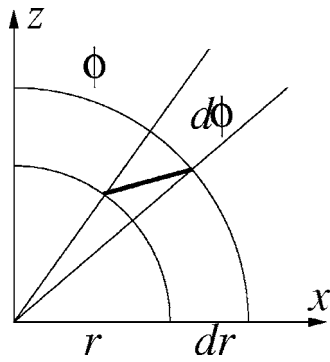
$$r = \sqrt{\frac{\Gamma}{4\pi}\frac{\sin\phi}{|\mathbf{u}|}}. \tag{A4}$$

The surfaces of constant speed are like toruses without an open center.

In order to compute the probability density function of $|\mathbf{u}|$, we introduce an intermediate variable l, where

$$|\mathbf{u}| = \frac{1}{l^2}, \quad l = r\sqrt{\frac{4\pi}{\Gamma\sin\phi}}. \tag{A5}$$

The variable l is used to avoid the coordinate transformation from two independent variables to one, i.e., $(r,\phi) \rightarrow |\mathbf{u}|$. The

FIG. 10. Calculation of length of a differential element in $r-\phi$ space.

pdf of $|\mathbf{u}|$ can now be found using a change of variables from $|\mathbf{u}|$ to l (see Ref. 34, p. 7),

$$p_1(|\mathbf{u}|)d|\mathbf{u}| = P[l(|\mathbf{u}|)]\left|\frac{dl}{d|\mathbf{u}|}\right|d|\mathbf{u}|. \tag{A6}$$

The particular form of l was chosen because of its geometric interpretation, which allows for the calculation of $P(l)$. Consider the volume bounded between two surfaces $l=l_1$ and $l=l_2$,

$$\frac{1}{V}\int_{l_1}^{l_2} A(l)dl, \tag{A7}$$

where $A(l)$ is the surface area of the torus. This volume gives the probability that a random point chosen from a sample volume in R^3 will be between the surfaces of constant l_1 and constant l_2.

In order to calculate $A(l)$, we must find the arc length of a constant l surface in the x-z plane, as shown in Fig. 10. The length of a differential element is $\sqrt{r^2d\phi^2+dr^2}$. The surface area of this strip, when rotated about the z axis, is

$$2\pi r\cos\phi\sqrt{r^2d\phi^2+dr^2}, \tag{A8}$$

where $2\pi r\cos\phi$ is the circumference of the circle around the z axis. Using the definition of a differential,

$$dr = \frac{dr}{d\phi}d\phi = \frac{l\cos\phi}{2\sqrt{4\pi\sin\phi}}d\phi. \tag{A9}$$

To find the total surface area for a fixed l, integrate strips of area around the torus in ϕ:

$$A(l) = \int_0^\pi 2\pi r\cos\phi\sqrt{r^2+\left(\frac{dr}{d\phi}\right)^2}d\phi \tag{A10}$$

$$= \int_0^\pi 2\pi l\sqrt{\frac{\sin\phi}{4\pi}}\cos\phi\sqrt{\frac{l^2\sin\phi}{4\pi}+\frac{l^2\cos^2\phi}{16\pi\sin\phi}}d\phi \tag{A11}$$

$$= \frac{1}{2}l^2\int_0^\pi \cos\phi\sqrt{\sin^2\phi+\frac{1}{4}\cos^2\phi}d\phi \tag{A12}$$

$$= c_1 l^2, \tag{A13}$$

where c_1 is a constant. So the probability density function for a randomly chosen point in R^3 in terms of l is $P(l)=c_1 l^2 dl$. Recalling that $l=|\mathbf{u}|^{-1/2}$, the probability density function of velocity magnitude is

$$p_1(|\mathbf{u}|)d|\mathbf{u}| = P(l(|\mathbf{u}|))\left|\frac{dl}{d|\mathbf{u}|}\right|d|\mathbf{u}| = \frac{c_1}{|\mathbf{u}|}\frac{1}{2|\mathbf{u}|^{1.5}}d|\mathbf{u}|$$

$$= \frac{c_2}{|\mathbf{u}|^{2.5}}d|\mathbf{u}|. \tag{A14}$$

The fact that the velocity pdf induced by a single point vortex is $p_1(|\mathbf{u}|)\sim 1/|\mathbf{u}|^{2.5}$ indicates that a velocity field with numerous point vortices in 3D QG is a Lévy law, as discussed in the text.

[1]B. Fornberg, "A numerical study of 2-D turbulence," J. Comput. Phys. **25**, 1 (1977).
[2]J. C. McWilliams, "The emergence of isolated and coherent vortices in turbulent flow," J. Fluid Mech. **146**, 21 (1984).
[3]G. F. Carnevale, J. C. McWilliams, Y. Pomeau, J. B. Weiss, and W. R. Young, "Evolution of vortex statistics in two-dimensional turbulence," Phys. Rev. Lett. **66**, 2735 (1991).
[4]J. C. McWilliams, J. B. Weiss, and I. Yavneh, "Anisotropy and coherent vortex structures in planetary turbulence," Science **264**, 410 (1994).
[5]J. C. McWilliams, "The vortices of geostrophic turbulence," J. Fluid Mech. **219**, 387 (1990).
[6]J. C. McWilliams, J. B. Weiss, and I. Yavneh, "The vortices of homogeneous geostropic turbulence," J. Fluid Mech. **401**, 1 (1999).
[7]A. Okubo, "Horizontal dispersion of floatable particles in the vicinity of velocity singularities such as convergences," Deep-Sea Res. **17**, 445 (1970).
[8]J. Weiss, "The dynamics of enstrophy transfer in two-dimensional hydrodynamics," Physica D **48**, 273 (1991).
[9]D. Elhmaïdi, A. Provenzale, and A. Babiano, "Elementary topology of two-dimensional turbulence from a Lagrangian viewpoint and single-particle dispersion," J. Fluid Mech. **257**, 533 (1993).
[10]M. Farge, N. Kevlahan, V. Perrier, and E. Goirand, "Wavelets and turbulence," Proc. IEEE **84**, 639 (1996).
[11]J. C. McWilliams, "The vortices of two-dimensional turbulence," J. Fluid Mech. **219**, 361 (1990).
[12]M. Farge and T. Philipovitch, "Coherent structure analysis and extraction using wavelets," in *Progress in Wavelet Analysis and Applications*, edited by Y. Meyer and S. Roques (Editions Frontieres, Gif-sur-Yvette, 1993), p. 477.
[13]A. Siegel and J. B. Weiss, "A wavelet-packet census algorithm for calculating vortex statistics," Phys. Fluids **9**, 1988 (1997).
[14]M. Farge, K. Schneider, and N. Kevlahan, "Non-Gaussianity and coherent vortex simulation for two-dimensional turbulence using an adaptive orthogonal wavelet basis," Phys. Fluids **11**, 2187 (1999).
[15]J. E. Ruppert-Felsot, O. Praud, E. Sharon, and H. L. Swinney, "Extraction of coherent structures in a rotating turbulent flow experiment," Phys. Rev. E **72**, 016311 (2005).
[16]C. Pasquero, A. Provenazale, and J. B. Weiss, "Vortex statistics from eulerian and Lagrangian time series," Phys. Rev. Lett. **89**, 284501 (2002).
[17]A. Provenzale, "Transport by coherent barotropic vortices," Annu. Rev. Fluid Mech. **31**, 55 (1999).
[18]J. C. McWilliams and J. B. Weiss, "Anisotropic geophysical vortices," Chaos **4**, 305 (1994).
[19]A. Bracco, J. von Hardenberg, A. Provenzale, J. B. Weiss, and J. C. McWilliams, "Dispersion and mixing in quasigeostrophic turbulence," Phys. Rev. Lett. **92**, 084501 (2004).
[20]J. B. Weiss, A. Provenzalea, and J. C. McWilliams, "Lagrangian dynamics in high-dimensional point-vortex systems," Phys. Fluids **10**, 1929 (1998).
[21]A. Bracco, J. LaCasce, C. Pasquero, and A. Provenzale, "The velocity distribution of barotropic turbulence," Phys. Fluids **12**, 2478 (2000).
[22]A. Bracco, J. H. LaCasce, and A. Provenzale, "Velocity probability density functions for oceanic floats," J. Phys. Oceanogr. **30**, 461 (2000).
[23]A. Bracco, E. P. Chassignet, Z. D. Garraffo, and A. Provenzale, "Lagrang-

ian velocity distributions in a high-resolution numerical simulation of the North Atlantic," J. Atmos. Ocean. Technol. **20**, 1212 (2003).

[24] J. G. Charney, *On the Scale of Atmospheric Motions* (Geofysiske Publikasjoner, 1948), Vol. 17, pp. 1–17. Republished in *The Atmosphere, a Challenge: The Science of J. Gregory Charney*, edited by R. S. Lindzen, E. N. Lorenz, and G. W. Platzman (AMS, Boston, MA, 1990).

[25] R. Salmon, *Geophysical Fluid Dynamics* (Oxford University Press, New York, 1998).

[26] J. Jeong and F. Hussain, "On the identification of a vortex," J. Fluid Mech. **285**, 69 (1995).

[27] Y. Dubief and F. Delcayre, "On coherent vortex identification in turbulence," J. Turbul. **1**, 111 (2000).

[28] F. Paparella, A. Babiano, C. Basdevant, A. Provenzale, and P. Tanga, "A Lagrangian study of the Antarctic polar vortex," J. Geophys. Res. **102**, 6765 (1997).

[29] P. R. Spalart, R. D. Moser, and M. M. Rogers, "Spectral methods for the Navier-Stokes equations with one inifinite and two periodic directions," J. Comput. Phys. **96**, 297 (1991).

[30] A. N. Kolmogorov, "A refinement of previous hypotheses concerning the local structure of turbulence in a viscous incompressible fluid at high Reynolds number," J. Fluid Mech. **13**, 82 (1962).

[31] R. H. Kraichnan, "Inertial ranges in two-dimensional turbulence," Phys. Fluids **10**, 1417 (1967).

[32] J. G. Charney, "Geostrophic turbulence," J. Atmos. Sci. **28**, 1087 (1971).

[33] I. Min, I. Mezić, and A. Leonard, "Lèvy stable distributions for velocity and velocity difference in systems of vortex elements," Phys. Fluids **8**, 1169 (1996).

[34] D. Sornette, *Critical Phenomena in Natural Sciences*, 2nd ed. (Springer, New York, 2004).

[35] A. Griffa, K. Owens, L. Piterbarg, and B. Rozovskii, "Estimates of turbulence parameters from Lagrangian data using a stochastic particle model," N.Z.J. Mar. Freshwater Res. **53**, 371 (1995).

[36] P. Falco, A. Griffa, P. Poulain, and E. Zambianchi, "Transport properties in the Adriatic Sea as deduced from drifter data," J. Phys. Oceanogr. **30**, 2055 (2000).

[37] M. Veneziani, A. Griffa, A. M. Reynolds, and A. J. Mariano, "Oceanic turbulence and stochastic models from subsurface Lagrangian data for the northwest Atlantic Ocean," J. Phys. Oceanogr. **34**, 1884 (2004).

[38] A. Griffa, L. I. Piterbarg, and T. Ozgokmen, "Predictability of Lagrangian particles trajectories: Effects of smoothing of the underlying Eulerian flow," N.Z.J. Mar. Freshwater Res. **62**, 1 (2004).

[39] C. Pasquero, A. Provenzale, and A. Babiano, "Parameterization of dispersion in two-dimensional turbulence," J. Fluid Mech. **439**, 279 (2001).